Journal of The Electrochemical Society

OPEN ACCESS

Bonded Bipolar Plate-Graphite Felt Components for Redox Flow Batteries Manufactured via Thermal Fusion by Electro-Welding

To cite this article: Wiebke Germer *et al* 2024 *J. Electrochem. Soc.* **171** 080535

Journal of The Electrochemical Society, 2024 **171** 080535

Bonded Bipolar Plate-Graphite Felt Components for Redox Flow Batteries Manufactured via Thermal Fusion by Electro-Welding

Wiebke Germer,[1,=,z] Barbara Satola,[2,=,z] Leif-Arvid Schillert,[3] Gaurav Gupta,[4,5] Lisa M. Uhlig,[1] and Nambi Krishnan N.[1]

[1]*German Aerospace Center (DLR), Institute of Engineering Thermodynamics, Oldenburg 26129, Germany*
[2]*German Aerospace Center (DLR), Institute of Networked Energy Systems, Oldenburg 26129, Germany*
[3]*Leif Schillert - Technische Planung und Beratung, Scheggerott 24392, Germany*
[4]*Resources Institute (TERI), Darbari Seth Block, Core 6C, India Habitat Centre, New Delhi-110 003, India*
[5]*Mission-Innovation India, Climate, Energy and Sustainable Technology, Department of Science & Technology, Technology Bhavan, New Delhi-110016, India*

Bipolar plates and graphite felt electrodes were thermally fused to one single component via a newly developed electro-welding process. A dropwise arrangement of the polymeric binder led to mechanically stable bonding and was documented by X-ray micro-computed tomography. Electrical conductivity of the fused components was achieved without any conductive filler and electro-welded samples show lower resistance values than unbonded ones at the same graphite felt electrode compression of 5% in ex situ electrical conductivity measurements. Applicability was demonstrated in situ in a 2-cell vanadium redox flow battery stack operated at a graphite felt electrode compression rate of 5% only. Obtained energy efficiencies of the battery are at least equal or even higher compared to state of the art vanadium redox flow battery with unbonded components at 20% graphite felt electrode compression. Composite components will simplify stack assembly and their increased electrode porosity during operation is expected to reduce pressure drop and to increase overall system efficiency.
 [DOI: 10.1149/1945-7111/ad6d96]

Manuscript submitted June 7, 2024; revised manuscript received July 31, 2024. Published August 23, 2024.

Energy from intermittent renewable sources entails the need for the development of innovative energy storage systems. Different alternatives are needed for various timescales of energy storage from short term to long term.[1–4] In this context, the principle of the redox flow battery (RFB) is an appealing variant, as it allows easy scaling of power and capacity independently.[2,5–8] RFBs consist of two electrolyte tanks whose volume directly correlates with the amount of energy that can be stored, and a stack of reaction cells which can be connected in series and scaled in size, thus, determining the power and current output. A chemical redox reaction is taking place in each cell for charging and discharging the battery by executing the same reversible reaction vice versa.[2]

Up to date, the most advanced flow battery type is the Vanadium Redox Flow Battery (VRFB) first described in the 1980's.[9] In addition, several new approaches have been published recently, e.g. organic flow batteries with water based electrolytes[10–16] or membrane free flow batteries.[17]

Due to these promising developments and the basically flexible buildup of flow battery systems, it is reasonable to shed light also on other general aspects of this technique. Inter alia, flow battery stacks contain bipolar plates (BPP) as current collectors and physical separators for the individual cells and porous graphite felt electrodes (GFE) responsible for distribution of the electrolyte pumped through the stack.[2,18]

Currently, flow battery stacks are assembled from their unbonded single components and then joined by an external frictional connection to ensure a sufficient electrical conductivity between the components.[2,18] Especially the flexible GFEs are compressed by an external force which affects their spatial structure. These changes in GFE porosity influence electrolyte flow and thus the energy efficiency (EE) of the battery.

Ghimire et al.[19] performed a comprehensive study on VRFB EE by varying the compression level of the porous electrode between 15%–40%. EE values were determined and contrasted with the pumping losses caused by pressure drop in highly compressed cells. As an optimum, a GFE compression rate of 20%–25% was found. The applied contact pressure ensures a sufficient electrical conductivity between unbonded GFE and BPP, as is state of the art. Also a significant influence of the compression rate on the pressure drop (ΔP) was shown which is directly proportional to the pumping energy.[20] An increase of ΔP up to circa 200% was reported for 40% felt compression. The study also shows that ΔP varies with the state of charge due to changes in the viscosity according to the oxidation state of the electrolyte. This fluctuation is more pronounced for high GFE compressions rates.[20] Also, the difference in ΔP between both half-cells is larger for higher compression rates. A smaller deviation in ΔP between the half-cells is favorable as this reduces the convective drag and the electrolyte crossover.[21]

As ΔP and electrical conductivity behave inversely to each other, the named optimum of 20% felt compression is in fact a compromise between these two parameters. Fused compound materials may generate the ability to overcome this dependency. The verification of sufficient electrical conductivity between GFE-BPP components by binding both materials in advance of battery assembly would allow the utilization of much lower compression forces. Thus, reduced ΔP due to higher GFE porosities and reduced pumping losses during battery operation should entail an increased overall system efficiency.[22] It is an effect that is even pronounced for larger stacks and larger system sizes.

Beyond that, further advantages may arise from optimizations in the up-to-date often custom-built stack manufacturing.[23] The usage of fused GFE-BPP components significantly reduces the overall number of components that are needed for stack assembly. It will simplify an industrial fabrication process of battery stacks and therefore not only lower production costs but also reduce malfunction sources.

Recently, we reported a first method to combine GFE and BPP for the usage in VRFB to one component by a thermal fusing procedure.[24] In the previous study, a hot-pressing process was applied and a mixture of polyvinylidene fluoride (PVDF) and a carbon-based conductive additive was utilized to unify the GFE and the BPP thus ensuring a conductive and mechanically stable connection. Comparable EE values to the state of the art (20% compression, unbonded components) were obtained by applying a compression rate of 5% only to a 2-cell VRFB. Thus, the above described advantages are applicable.

[=]Equal Contribution.
[z]E-mail: wiebke.germer@dlr.de; barbara.satola@dlr.de

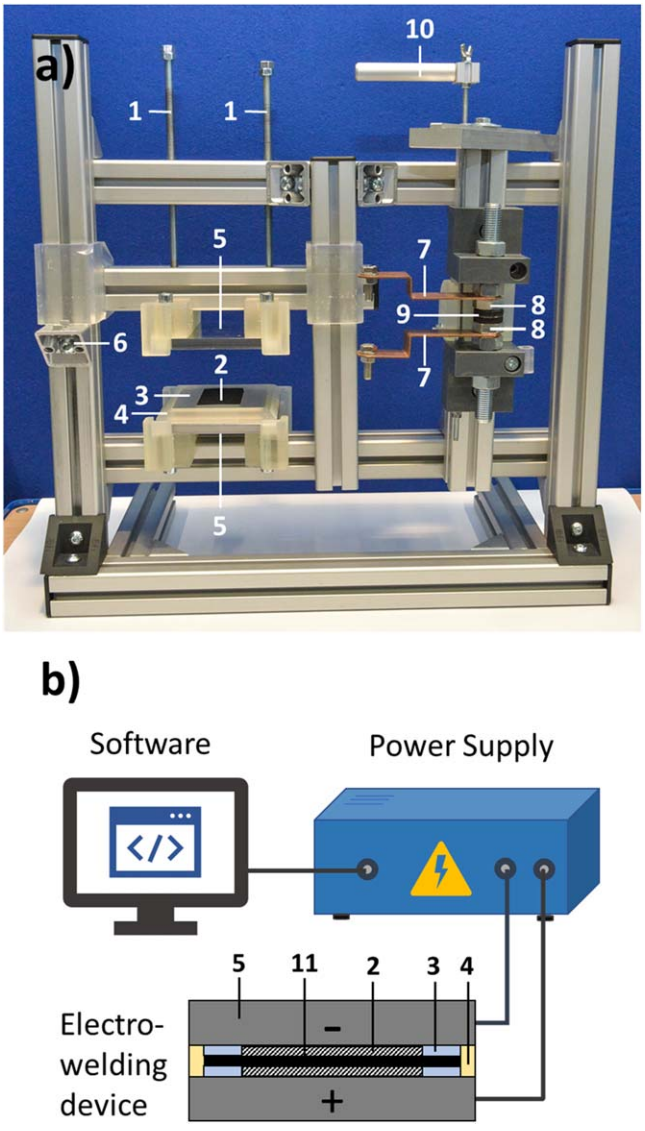

Figure 1. Inhouse designed welding device for different sample sizes on laboratory scale—in situ stack size (left) and ex situ sample sizes (right) (a), schematic build-up (b). Threaded rods for adjustment of contact pressure (1), graphite felt electrode (GFE) (2), inner non-electroconductive frames for GFE positioning (3), outer non-electroconductive frames/spacers (4), contact metal plate (5), screw for adjustment of upper contact metal plate height (6), connection plate from contact plates to power supply (7), contact metal plates (8), sandwiched sample (9), lever for height adjustment of right welding device (10), bipolar plate (BPP) (11). The PVDF powder is spread below and above the BPP, id est in between the BPP (11) and the GFE (2).

In the present work, an additional thermal fusing method via electro-welding is presented. The individual components GFE and BPP were successfully combined to bonded GFE-BPP and GFE-BPP-GFE. Compared to the first published hot-pressing method this new method is faster and simpler in application and allows full omission of conductive fillers (often graphite based *nano*-materials). It provides a significant improvement with respect to number of production steps, costs, operational safety and environmental health.

Methods

GFE-BPP and GFE-BPP-GFE materials and pretreatment.— Composite BPPs containing 85% graphite and 15% PVDF (Sigracell PV15, SGL Carbon SE, Germany) and polyacrylonitrile (PAN) based GFE (Sigracell GFD 4.6 EA, SGL Carbon SE, Germany) were utilized for this investigation. Samples were cut into the respective sizes (conductivity measurement: diameter of a circle of 25 mm for BPP and GFE; X-ray micro-computed tomography (μ-CT): diameter of a circle of 16 mm for BPP and 11 mm for GFE; VRFB stack: 86 mm x 74 mm for BPP and 60 mm x 40 mm for GFE). BPPs were cleaned with deionized water and ethanol before use. GFEs were thermally activated by the supplier and used as received. PVDF powder (1.54 mg cm^{-2}) (Solef 6010/001, Solvay GmbH, Germany) was used as bonding material between the BPP and GFE since the composite BPP already contains the same type of polymer.

Electro-welding of GFE-BPP and GFE-BPP-GFE components.—For the fusion of the GFE and the BPP an inhouse developed electro-welding procedure was employed (Fig. 1). For in situ operation in a VRFB and for ex situ characterization different sample sizes were required, as described above. For the in situ samples inner non-electroconductive frames were used to ensure a centered placement of the GFEs on the BPP. The components were sandwiched to either GFE-BPP or GFE-BPP-GFE stacks with manually distributed PVDF powder at their single interface. For the sandwiched components consisting of GFE-BPP-GFE, PVDF was added to one side of the GFE in a first step and covered with the BPP. In a second step PVDF was applied to the top side of the BPP, then the second GFE was placed on top. The sandwiched samples were placed in outer non-electroconductive frames within the electro-welding device. Main constituents of the apparatus are vertically adjustable contact metal plates made from stainless steel with suitable dimensions mounted in the inhouse constructed welding device as shown in Fig. 1a. Threaded rods allowed adjustment of precise contact pressure of the unfused components at the start of the welding process. Additionally, the outer non-electroconductive frames served also as spacers between the contact plates and thus ensured that the GFE was not compressed above 5%. Then, a direct current was applied vertically to the stacked components for a defined time span (Fig. 1b). Source-Sink Series NL (Höcherl & Hackl GmbH, Germany) was used as power supply. Both the current and fusion time were gradually varied for iterative process optimization. E.g. a current density of 3.5 A cm^{-2} for several seconds lead to appropriate fusion results. More details are found in the results chapter "Electro-welding process control." Electrical current, resistance and power were measured between the contact plates with a VC840 digital multimeter (Voltcraft, Germany) and recorded throughout the fusion process. Controlling of the welding process and data acquisition was carried out via an inhouse designed software tool.

Electrical conductivity.—A zwickiLine Z1.0 single-column materials testing machine (ZwickRoell GmbH & Co. KG, Germany) in combination with a DMM 4050 6–1/2 Digit Precision Multimeter (Tektronix Inc., USA) was used to measure the electrical through-plane resistance of bonded and unbonded GFE-BPP-GFE. The stacked samples were inserted between two gold plated copper stamps (d = 2.5 cm) for the measurement. The respective force for 5% and 20% GFE compression was adjusted by the measurement device.

The overall electrical through-plane resistance measured consists of the following contributions (Eq. 1):[24]

$$R_E = 2R_{Au(Cu)-GFE} + 2R_{GFE} + 2R_{GFE-BPP} + R_{BPP} \quad [1]$$

Where R_E gives the total electrical through-plane resistance, $R_{Au(Cu)-GFE}$ is the contact resistance between a gold plated copper stamp and the GFE, R_{GFE} is the bulk resistance of the GFE, $R_{GFE-BPP}$ is the contact resistance between GFE and BPP and R_{BPP} is the bulk resistance of the BPP.

X-ray micro-computed tomography (μ-CT).—μ-CT images of the electro-welded components were produced with a SkyScan 1172 computed tomography scanner (Bruker, Belgium) with a source voltage of 80 kV. The samples were placed in a 3D printed

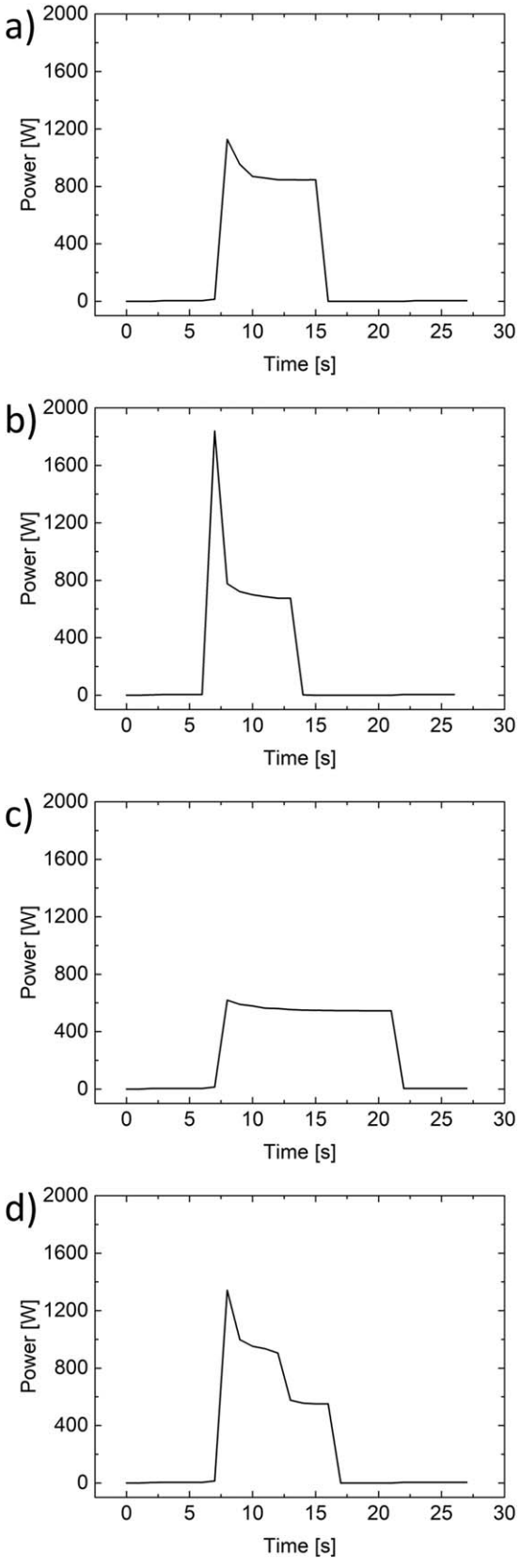

Figure 2. Different power-time-curves of welding processes by applying 3.5 A cm^{-2} to samples with dimensions for in situ battery application. Successful (a)–(c) and not successful fusion attempts (d).

polypropylene housing to simulate in situ GFE compression rate of 5%. In the μ-CT they were rotated from 0° to 180° with rotation step of 0.18°. The scan resolution was 1.64 μm and cross-section gray scale images were gathered as an average of 6 frames at each rotation step. Recorded gray scale image data was reconstructed in the NRecon software (Bruker, Belgium) by keeping the range of the gray scale histogram, ring artefact reduction and beam hardening identic for all samples. Subsequently, filtering and despeckling operations were carried out with the CTAn software (Bruker, Belgium) to eliminate background noise followed by a segmentation of the region of interest into white (matter) and black (background).

VRFB assembly and testing.—Fused components were investigated in situ in a specially designed 2-cell VRFB short stack (Schmid Group, Germany) with two different frame sets to achieve the respective rate of 5% or 20% GFE compression and with copper plates as current collectors. The active cell area was 24 cm^2. Nafion 117 (QuinTech, Germany) was used as separator and the membrane was cleaned in 10% H_2O_2 for 30 min at 80 °C before use. A volume of 100 ml of vanadium electrolyte (1.6 M $V^{3+/4+}$ (50%:50%; V^{3+}:V^{4+}) / 4 M SO_4^{2-}, GfE Metalle und Materialien GmbH, Germany) were utilized for the positive and negative half-cell, respectively. The electrolyte was constantly purged with nitrogen and cyclically pumped (Simdos 10, KNF Neuberger GmbH, Germany) through the short stack at a flow rate of 60 ml min^{-1}. Stack operation was carried out at room temperature and data acquisition was conducted by a Solartron Analytical 2100 A potentiostat (Ametek Scientific Instruments, USA). One hundred charge/discharge cycles were performed at a current density of 80 mA cm^{-2} and charge/discharge cut off voltages were set to 3.2 V and 1.6 V, respectively. EE of the stack was calculated.[25,26]

Results and Discussion

Preliminary considerations and electro-welding tests.—The idea behind electro-welding of stacked GFE-BPP and GFE-BPP-GFE materials is that they can be fused in only one single work step, as electro-welding allows the internal bonding of components across a 2-dimensional interfacial area that is not directly accessible from the outside. While the current is induced, the temperature rises at the interface between the single components due to their contact resistance which provokes the melting of the PVFD powder and thus leads to a mechanical stable bonding after cooling. As the developed temperature rise is limited solely to the interface area, the polymer in the bulk of the composite BPP is not significantly affected and the precise dimensions of the BPP remain unchanged.

The newly developed electro-welding method was successfully applied to produce bonded GFE-BBP and GFE-BPP-GFE components within a couple of seconds of fusion time. The bonding is mechanically stable and no delamination of the GFE was observed after successful fusion. As no additional chemical substance was used to achieve this connection besides PVDF which is part of the BPP compound material itself, it is assumed that the chemical stability of the compound is equal to the individual materials. This is of great importance, especially for VRFB application, as the sulfuric vanadium electrolyte is a very corrosive environment. Also, it has to be ensured that the additional fusion layer does not affect the electrical conductivity between the GFE and BPP negatively during operation, e.g. due to isolating properties of the used polymer. Thus, the application of an as small as possible amount of polymer is favorable. The PVDF amount could be lowered to 1.54 mg cm^{-2} while still ensuring a mechanically stable bonding. The fused components were characterized ex situ by electrical conductivity measurements and μ-CT-analysis as well as in situ by VRFB application in a 2-cell stack.

Figure 3. Deposition on welding electrodes after charring of samples during poor fusion attempt.

Electro-welding process control.—During method development current density set values were increased stepwise while monitoring actual current and voltage values. Tests starting at a current density value of 0.8 A cm^{-2} until a value of 3.5 A cm^{-2} was found to yield in mechanically stable fusion results, whereas higher values lead to charring of the samples. Analysis of the collected data revealed as most relevant finding that the power vs time curve of the source sink exposes a maximum peak at the beginning of the welding process. Here, it has been noticed that a minimum value of 500 W is required for successful welding of the samples. Figure 2a displays a characteristic power-time-curve for a successful fusion process. The height of the initial peak typically varies over a range from 700 W to 1100 W, but can also reach sharp maximum peaks of 1900 W (Fig. 2b) as well as rather flat peaks around 600 W only (Fig. 2c). In all described cases the initial peak is followed by an asymptotic decrease to a plateau at about 500 W to 800 W. Probably, deviations in the primary materials utilized as well as in the manually performed production process, e.g. the distribution of PVDF powder on the interfaces of the sandwiched samples, can be listed as causes for these varying curve progressions. In the beginning of the development of this new method the fusion current density (3.5 A cm^{-2}) was applied for time spans of >40 s which lead to proper results. Interpretation of the power-time-curves suggested that the fusion is completed when the plateau is reached. Subsequently it could in fact be shown that the shortening of the fusion time to <10 s also led to stable compound materials.

However, under some circumstances the appearance of a second plateau was observed (Fig. 2d). In fusion attempts that display this second plateau, organic material was charred and deposited on the metallic electrode plates (Fig. 3). Consequently, the fusion was not successful. The electrode plates had to be cleaned thoroughly before they were used again, otherwise the electric conductivity ratio between plates and sample was altered. To eliminate this non-desirable behavior in the future it is planned to include a software control mechanism that detects the first plateau and accordingly aborts the welding process. A mere break-off after a specific time span seems not to be sufficient as the asymptotic decrease is pronounced to different degrees and the time span of the plateau varies from 2 s to 10 s, whereas the second unwanted power drop-off can already appear after e.g. 5 s.

Electrical conductivity.—The electrical conductivity of electro-welded GFE-BPP-GFE samples (labeled as EW) was compared to unbonded one (labeled as UB). Additionally, results from GFE-BPP-GFE samples that were recently obtained by our working group via a hot-pressing method (labeled as HP),[24] are included for comparison reasons (Fig. 4). One obvious finding during the development of the hot-pressing method was the severe increase of the resistance of the fused HP components by adding only the binding polymer to the

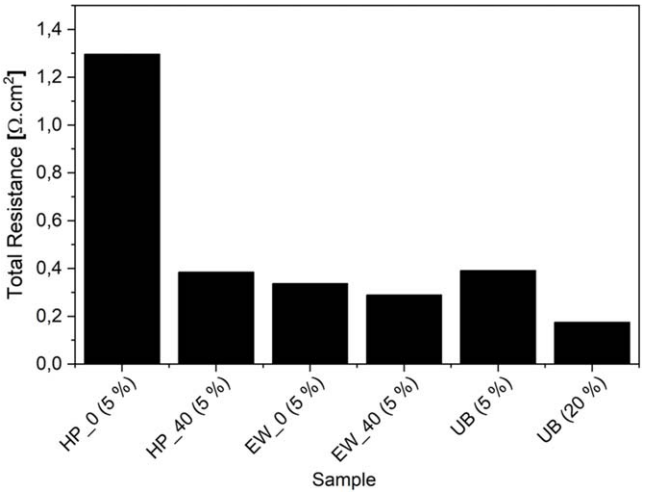

Figure 4. Electrical resistance of different thermally fused samples at 5% compression—hot-pressed samples without conductive filler HP_0 (5%) and with 40% carbon black HP_40 (5%),[24] electro-welded sample without conductive filler EW_0 (5%) and with 40% carbon black EW_40 (5%); unbonded samples UB (5%) and UB (20%) at 5% and 20% compression, respectively.

interface. Therefore, conductive fillers were added and a mixture of 40% conductive carbon black in proportion to PVDF was found most beneficial to lower electrical resistance of the fused HP components to roughly 1/3 of the former value.[24] In order to investigate this electrical conductivity effect also on the EW samples, they were either prepared with only PVDF or with a mixture of carbon black and PVDF as well. The respective percentual amount of carbon black is labeled as "0" or "40" within the sample name in Fig. 4 where the total resistances of various HP and EW fused components at 5% compression and of UB components at 5% and 20% compression are shown. HP and EW samples were generally prepared in the same manner for both methods and equal in materials, size, and preparation. However, the amount of PVDF that is necessary to achieve a mechanically stable connection could be lowered for the welding process (1.54 mg cm^{-2} compared to 2.08 mg cm^{-2}).

With respect to the strong isolating effect of PVDF observed by the HP samples, it is a surprising finding that EW components without conductive filler achieve even lower resistance values than the HP components with 40% carbon black. By preparing the EW sample like the HP ones with 40% carbon black at the interface the resistance could indeed be lowered further, but not that significantly. Both EW samples and the HP_40 (5%) show lower resistance values

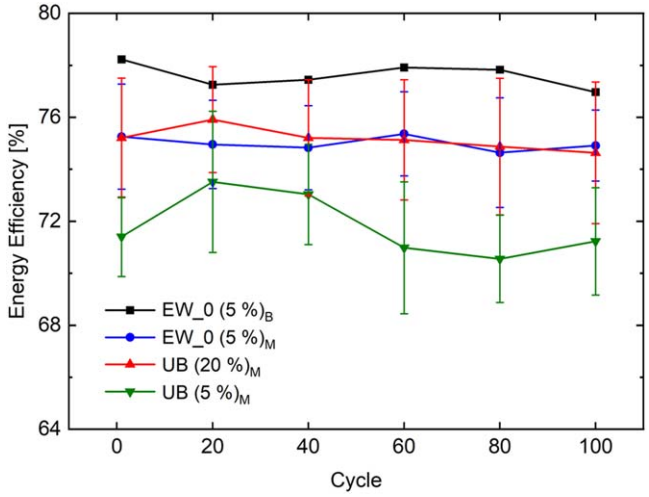

Figure 5. Energy efficiencies of a 2-cell VRFB (100 charge/discharge cycles, 80 mA cm^{-2}) using either unbonded or electro-welded GFE and BPP samples. Mean values at 5% GFE compression are given for electro-welded components without conductive fillers (EW_0 $(5\%)_M$ – 5 samples welded at 3.5 A cm^{-2}) and for unbonded components (UB $(5\%)_M$ – 4 samples), as well as unbonded components at 20% GFE compression (UB $(20\%)_M$ – 6 samples). EW_0 $(5\%)_B$ depicts the best performing electro-welded sample (0% carbon black, 1.54 mg/cm^2 PVDF powder, 3.5 A cm^{-2} welding current, VRFB operated with 5% GFE compression).

at the same GFE compression of 5% when compared to UB (5%). Only the highly compressed UB (20%) achieves better electrical conductivity, however, it leads to loss of GFE porosity.

As an undesired effect, the addition of carbon black at the interface between the GFE and BPP of sample EW_40 could potentially promote the evolution of hydrogen during charging in the negative half-cell of a vanadium redox flow battery in contrast to sample EW_0.[27] Furthermore, the absence of nano-particles (like e.g. conducting carbon powders) is highly favorable in an industrial process due to operational safety, avoidance of additional costs and environmental health. Therefore, the electro-welded component EW_0 which is free of conductive additives was chosen for further evaluation and battery efficiency testing.

VRFB assembly and testing.—Samples of the EW_0 component were operated in situ at a GFE compression rate of 5% in a 2-cell VRFB stack to evaluate the performance in flow battery application. The results are examined and compared to the state of the art of UB components with 20% GFE compression, as well as to UB components at 5% GFE compression rate. The setup of a 2-cell stack was chosen in order to test both GFE-BPP and GFE-BPP-GFE electro-welded components. The VRFB stack was run for 100 cycles at 80 mA cm^{-2} to assess the stability of the electro-welded components during operation.

Results of the battery test in Fig. 5 are given as mean values of multiple samples to demonstrate the reproducibility of the installed setup and of the newly developed electro-welding method itself. With this test setup an EE of roughly 75% was achieved for stacks with UB components at a GFE compression rate of 20% (UB $(20\%)_M$) which resembles the state of the art. Typically, EE values at current densities of 80 mA cm^{-2} are ranging roughly between 72%–83%.[28] However, the battery performance is a sum of different parameters, such as the operating conditions, the electrolyte concentration and composition as well as the application of single components and their interaction. For instance, the compression of the GFE within a single flow cell has a critical influence on the overall EE. Park et al.[22] have evaluated the EE of a VRFB single cell by varying the compression of the GFE. They reported energy efficiencies of 70.4%, 77.5%, 79.1% and 76.1% at a current density

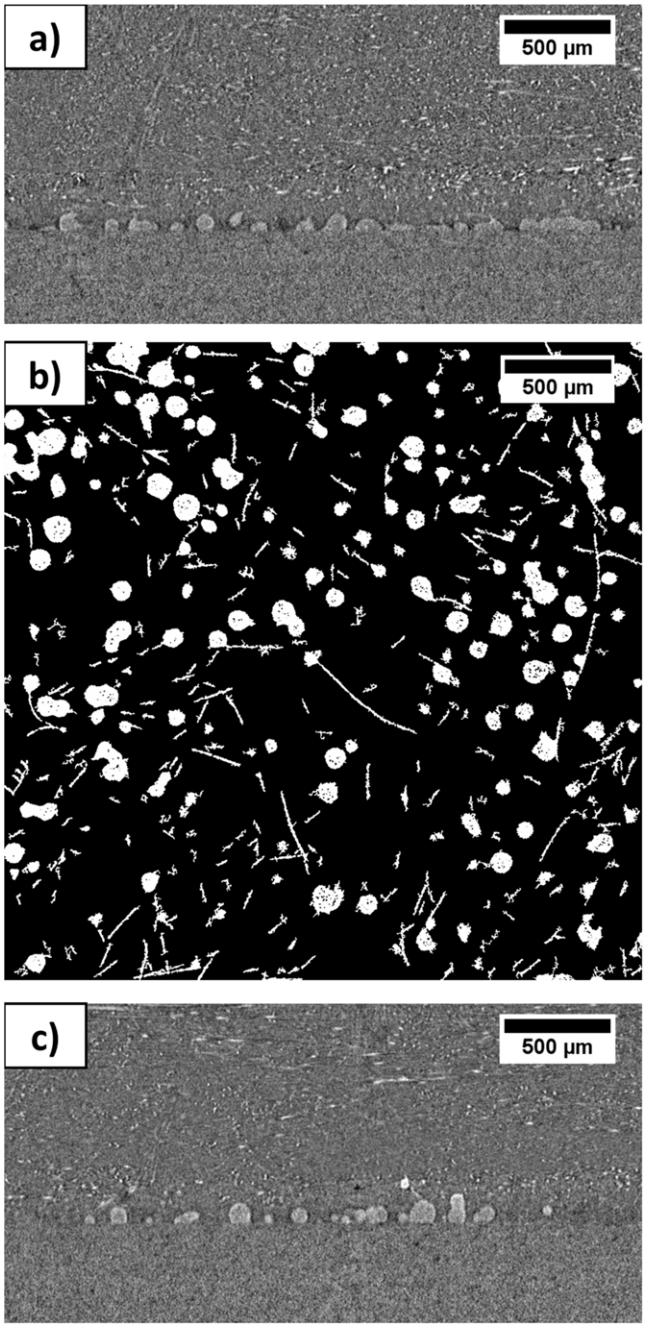

Figure 6. Micro computed tomography images of the boundary region of EW_0 (5%) components. 2D coronal plane image (a) and 2D axial plane image (b) of the GFE-BPP interface of a pristine sample. 2D coronal plane image after 100 cycles of VRFB operation (c).

of 70 mA cm^{-2} when applying GFE compressions of 0%, 10%, 20% and 30%, respectively. Thus, in good agreement with the literature results, the reduction of the GFE compression rate to 5% applied to UB components (UB $(5\%)_M$) in the present research paper led expectedly to a decrease in EE to approximately 72%.

The 2-cell stack using EW_0 components at 5% GFE compression (EW_0 $(5\%)_M$) achieves a mean EE value of roughly 75% which is in the same range like the UB $(20\%)_M$. Samples prepared by the same fusion current density (3.5 A cm^{-2}) were used for calculating the mean value of EW_0. Although the welding duration was slightly varied for these samples in the range of half a minute, similar EE were obtained. Thus, it is shown that already at this early stage of development comparable EE results to the state of the art are

achieved. The EW_0 components show an equally stable performance over 100 cycles of VRFB testing just like the UB ones. To point out the potential of this new method the best performing sample with an EE of 78% is shown (EW_0 $(5\%)_B$ in Fig. 5) which is a plus of 3% in the EE of the battery compared to the mean value of the state of the art battery but under a significantly lower GFE compression rate. It means that additional benefits in the overall system efficiency are to be expected due to reduced pressure drop and pumping losses. It is likely, that further increases in the efficiency of the VRFB might be achievable by further optimizing the fabrication process which is up to now proceeded fully manually. Additionally, to enhance the production of flow batteries, fused components can potentially contribute to simplification and cost reduction in industrialized stack building.

As the basic chemical composition of the GFE and BPP was not affected during the electro-welding process and PVDF as one constituent of the BPP composite material was chosen as binding material at the interface, no significant alterations in the degradation behavior are expected during battery operation. This assumption could be confirmed by comparing the EE over time of bonded and unbonded components in the experimental battery setup. In order to visualize the morphology of the interface of pristine and aged samples and thus provide further evidence for (electro-)chemical stability μ-CT analysis was performed and is described in the following section.

μ-CT.—μ-CT imaging was conducted with EW_0 samples in pristine state and after operation in the VRFB 2-cell stack. In order to simulate mechanical stack conditions 5% compression of the GFE was applied during the μ-CT measurements. Figure 6 shows that fusion of the GFE and BPP is realized by an arrangement of small dots of the polymer between the two components. The 2D coronal plane image (Fig. 6a) displays a vertical cut through the layers of a freshly fused pristine sample, where the GFE is in the upper half of the picture and the BPP at the bottom. Recognizable in the border region in the middle are PVDF droplets with a particle size varying in the range of 30-180 μm, mainly between 80-90 μm. The horizontal cut through the border region given in the 2D axial plane image in Fig. 6b of a pristine sample confirms the conception of a dropwise arrangement of PVDF (white: matter, black: background). This distinct distribution is a result of the low overall amount of polymer and the brief application times of the welding current. The grouping of polymer-containing and polymer-free segments results in a suitably mechanical stable connection and sufficient electrical conductivity as well. Figure 6c depicts a vertical image section of an in situ aged EW_0 sample after 100 cycles of operation in a VRFB 2-cell stack. No significant changes in the structure or the bonding become visible in μ-CT examination. PVDF particle agglomeration does not occur during electro-welding process or performed battery operation.

In our previous report on hot-pressing procedure,[24] the entire bulk material had to be heated as a whole for a significant period of time (10–12 min), which was inevitable for transferring heat from the outer heating plates to the interfacial layer at the center of the workpiece. This led to a more laminar melting of the PVDF and thus resulted partly in a kind of widespread layer of the non-conducting polymer material. Therefore, in case of the hot-pressing method, the addition of conductive fillers was needed. In comparison to the electro-welding process the crucial difference is that the increase of temperature directly occurs at the interfacial region because it originates from an inhibited electric current flow from GFE to BPP. Thus, the contact area is heated selectively for a very brief time span, which leads to the desired uniform distribution of PVDF polymer as droplets at the GFE and BBP interface.

Conclusion and Outlook

This study demonstrates the manufacturing of an electrically conductive, mechanically and chemically stable bonding of GFE and BPP for VRFB stack application. It is realized via thermal fusion carried out by a newly developed electro-welding process. In a fast procedure by applying only a few seconds of welding current single components are combined to GFE-BPP and GFE-BPP-GFE units through a simple constructive build-up.

Operation of 100 charge/discharge cycles in a 2-cell VRFB stack with the newly developed components proved the feasibility in flow battery application. The morphology of the interface from μ-CT characterization showed uniformly distributed little droplets of PVDF holding together the fused components which remained unchanged after battery cycling. The mean EE during the battery operation was stable and comparable to stacks with unbonded components (2-cell stacks using either EW_0 $(5\%)_M$ or UB $(20\%)_M$ samples achieve a mean EE value of roughly 75%). Beyond that, an improvement of the EE of the battery stack with electro welded components up to 3% could be achieved under a GFE compression rate of 5% only compared to the state of the art (mean value at 20% GFE compression and unbonded components). The significantly reduced GFE compression which could be successfully demonstrated in battery operation implies higher porosity, lower pumping losses and increased overall system efficiency.

Conductive fillers are explicitly not needed in the described method to fabricate ready-to-operate compound materials. The electro-welded connection is achieved without the usage of further chemical substances that are not used in the starting materials anyway and hence the chemical resistivity is alike to the well-established single components. The usage of fused components offers the prospect to shorten and simplify the up to date predominantly manually carried out stack assembling process.

The authors plan a scale up to larger stack sizes and the determination of actual pressure drop rates under use of fused components. Furthermore, an optimized software control of the electro-welding process with automated abort criterions is considered.

Acknowledgments

The project “Research, Development and Evaluation of a Fusion Method for Realization of Integrated Bipolar Plate-Felt components for Redox-Flow-Batteries” (IBiFi—Fkz. 03ET6136C) was funded by the German Federal Ministry for Economic Affairs and Energy under the 6th Energy Research Programme “Research for an environmentally friendly, reliable and affordable energy supply.”

ORCID

Barbara Satola https://orcid.org/0000-0002-5807-1763
Nambi Krishnan N. https://orcid.org/0000-0002-3563-050X

References

1. X. Luo, J. Wang, M. Dooner, and J. Clarke, *Appl. Energy*, **137**, 511 (2015).
2. J. Girschik, L. Kopietz, M. Joemann, A. Grevé, and C. Doetsch, *Chem. Ing. Tech.*, **93**, 523 (2021).
3. B. Dunn, H. Kamath, and J.-M. Tarascon, *Science*, **334**, 928 (2011).
4. M. Sterner and I. Stadler, *Energiespeicher - Bedarf, Technologien, Integration* (Springer Vieweg Berlin, Heidelberg) (2017), 56*ff*.
5. D. H. Doughty, P. C. Butler, A. A. Akhil, N. H. Clark, and J. D. Boyes, *Electrochem. Soc. Interface*, **19**, 49 (2010).
6. T. Nguyen and R. F. Savinell, *Electrochem. Soc. Interface*, **19**, 54 (2010).
7. G. L. Soloveichik, *Chem. Rev.*, **115**, 11533 (2015).
8. M. Park, J. Ryu, W. Wang, and J. Cho, *Nat. Rev. Mater.*, **2**, 16080 (2016).
9. M. Skyllas-Kazacos, M. Rychcik, R. G. Robins, A. G. Fane, and M. A. Green, *J. Electrochem. Soc.*, **133**, 1057 (1986).
10. J. Winsberg, T. Hagemann, T. Janoschka, M. D. Hager, and U. S. Schubert, *Angew. Chem. Int. Ed.*, **56**, 686 (2017).
11. B. Yang, L. Hoober-Burkhardt, F. Wang, G. K. Surya Prakash, and S. R. Narayanan, *J. Electrochem. Soc.*, **161**, 1371 (2014).
12. K. Lin et al., *Science*, **349**, 1529 (2015).
13. R. M. Darling, K. G. Gallagher, J. A. Kowalski, S. Ha, and F. R. Brushett, *Energy Environ. Sci.*, **7**, 3459 (2014).
14. A. Ejigu, P. A. Greatorex-Davies, and D. A. Walsh, *Electrochem. Comm.*, **54**, 55 (2015).

15. T. Liu, X. Wei, Z. Nie, V. Sprenkle, and W. Wang, *Adv. Energy Mater.*, **6**, 1501449 (2016).
16. X. Wei et al., *Angew. Chem. Int. Ed.*, **54**, 8684 (2015).
17. P. Navalpotro, J. Palma, M. Anderson, and R. Marcilla, *Angew. Chem. Int. Ed.*, **56**, 12460 (2017).
18. P. Qian, H. Zhang, J. Chen, Y. Wen, Q. Luo, Z. Liu, D. You, and B. Yi, *J. Power Sources*, **175**, 613 (2008).
19. P. C. Ghimire, A. Bhattarai, R. Schweiss, G. G. Scherer, N. Wai, and Q. Yan, *Appl. Energy*, **230**, 974 (2018).
20. P. C. Ghimire, "Electrode modification and in situ studies to enhance the performance of vanadium redox flow batteries." *Thesis* (2019), Singapore, 128ff.
21. K. W. Knehr and E. C. Kumbur, *Electrochem. Comm.*, **23**, 76 (2012).
22. S.-K. Park, J. Shim, J. H. Yang, C.-S. Jin, B. S. Lee, Y.-S. Lee, K.-H. Shin, and J.-D. Jeon, *Electrochim. Acta*, **116**, 447 (2014).
23. B. R. Chalamala, T. Soundappan, G. R. Fisher, M. R. Anstey, V. V. Viswanathan, and M. L. Perry, *Proc. IEEE*, **102**, 976 (2014).
24. N. N. Krishnan, G. Gupta, B. Satola, L. M. Uhlig, W. Germer, and M. Zobel, *J. Electrochem. Soc.*, **169**, 100517 (2022).
25. G.-J. Hwang and H. Ohya, *J. Membrane Sci.*, **132**, 55 (1997).
26. L. D. Brown, T. P. Neville, R. Jervis, T. J. Mason, P. R. Shearing, and D. J. Brett, *J. Energy Storage*, **8**, 91 (2016).
27. K. Köble, M. Schilling, L. Eifert, N. Bevilacqua, K. F. Fahy, P. Atanassov, A. Bazylak, and R. Zeis, *ACS Appl. Mater. Interfaces*, **15**, 46775 (2023).
28. B. Satola, *J. Electrochem. Soc.*, **168**, 060503 (2021).